Contactless 3D surface characterization of additive manufactured metallic components using terahertz time-domain spectroscopy

YUEZHEN LU, HAITAO ZHU, ABDULLAH M. ZAMAN, ALLAN E. W. RENNIE, HUNGYEN LIN, YINGTAO TIAN, AND RICCARDO DEGL'INNOCENTI*

School of Engineering, Gillow Avenue, Lancaster University, Bailrigg, Lancaster LA1 4YW, United Kingdom
*r.deglinnocenti@lancaster.ac.uk

Abstract: Terahertz time-domain spectroscopy has experienced significant progress in imaging, spectroscopy, and quality inspection, e.g., for semiconductor packaging or the automotive industry. Additive manufacturing alloys (also known as alloys for use in 3D printing) have risen in popularity in aerospace and biomedical industries due to the ability to fabricate intricate designs and shapes with high precision using materials with customized mechanical properties. However, these 3D-printed elements need to be polished thereafter, where the surface roughness is inspected using techniques such as the laser scanning microscope. In this study, we demonstrate the use of terahertz time-domain spectroscopy to assess the average roughness profile and height leveling of stainless steel for comparisons against the same parameters acquired using laser scanning microscopy. Our results highlight the potential of the proposed technique to rapidly inspect 3D-printed alloys over large areas, thus providing an attractive modality for assessing surface profiles of AM-manufactured terahertz components in the future.

Published by Optica Publishing Group under the terms of the Creative Commons Attribution 4.0 License. Further distribution of this work must maintain attribution to the author(s) and the published article's title, journal citation, and DOI.

1. Introduction

Terahertz (THz) radiation is a portion of the electromagnetic spectrum situated between microwaves and infrared with frequencies between 0.1-10 THz, corresponding to vacuum wavelengths between 30-3000 µm. Interest in the THz range has experienced an exceptional growth in the latest years, due to the increased maturity of this technology as well as to the strategic importance of unique applications at this frequency range such as imaging and spectroscopy [1], biological applications [2], next generation wireless communications [3,4] and contactless non-destructive industrial applications [5]. This progress has been in part enabled by the developments made in compact THz sources, such as resonant tunneling diodes [6], quantum cascade lasers [7], as well as the increased efficiency, robustness and versatility of THz time-domain spectrometers (THz-TDS) [8]. It is these latter THz systems that have demonstrated suitability for spectroscopic and industrial applications, e.g. in the automotive and aerospace sectors [9], pharmaceutical [10] and semiconductor packaging quality control [11,12]. The non-ionizing nature of THz radiation is particularly attractive in manufacturing quality control, where unlike X-rays, can be realized without posing as a health hazard to the operating personnel. This has motivated numerous industrial applications. For example, THz-TDS has been used as an effective tool in revealing sub-surface features in multi-layers structures in optically opaque dielectrics [13] and polymers [14,15], measuring the electrical conductivity in semiconductors [16,17], characterizing the crystallization of polymer [18,19], extracting charge transfer speed in electronics [20], and investigating states of water in polymers [21].

#496166 https://doi.org/10.1364/OME.496166
Journal © 2023
Received 24 May 2023; revised 2 Aug 2023; accepted 2 Aug 2023; published 9 Aug 2023

Optical Materials EXPRESS

Nevertheless, most of these experiments were conducted on samples with smooth surfaces, without taking scattering into account. This is a topic that drawn interests fundamentally [22–33]. Scattering is strongly related to the surface average roughness (R_a) [22–25], which is an important limiting factor for THz measurements. Frequency-dependent amplitude changes resulting from specular reflections were correlated to the surface roughness for metallic surfaces, using Fourier transform far-infrared systems [23] and THz-TDS sources [24], dielectrics [28–30] and coatings [31]. In dielectric materials, the frequency dependence of the scattering losses can negatively affect specific spectral features, e.g. in explosives [28]. Hence, more complex theoretical models were proposed, by using wavelet analysis [29] or cepstrum filtering [30], to tackle this issue. Scattering is one of the ultimate limits for the development of efficient integrated THz platforms as well. THz miniaturized components and waveguides have been realized with several approaches [34–43], from surface plasmons [35], to micromachining [36,37], hollow waveguides [38], photonic crystals [39], 3D printing [40–42] and Additive Manufacturing (AM) [43].

Additive Manufacturing is a cutting-edge technique popular for simplifying the fabrication of complex design geometries in modern manufacturing. Selective laser melting (SLM) is one AM method used to fabricate components from metal feedstock materials with high density and excellent properties by utilizing a laser to selectively melt metal powder [44,45]. Metallic samples prepared by SLM suffer from poor surface uniformity due to the surface laser effects, which prohibit applications in biomedical devices and aerospace industry where a perfect control of surface profile is required [46–48]. To overcome this problem, Mohammad et al. and Han et al. have reported that electrochemical polishing (EP) can be applied as an effective additional step to remove surface imperfection using an environmental-friendly solvent [49,50]. Many techniques have been proposed to characterize R_a, such as contact scanning profilometry [51,52], X-ray micro-CT [53], atomic force microscope (AFM) [54] and laser scanning microscope [55] etc. However, most of these techniques are time-consuming where a complete range scanning is required but also facing the challenge of losing data at the peak and valley areas on the rough surface as they are out of the measuring limitation. In general, the R_a values of as-fabricated SLM samples are in the range of 25-100 μm, which is not within the range normally covered by these techniques. Thus, a more effective technique designed for evaluating the surface where R_a is in the range of tens of μm is required.

THz radiation has not previously been used to inspect the surface roughness on AM alloy components realized via SLM. Here, we exploit its sensitivity to scattering to extract the surface roughness distribution and height levelling (HL) allocation of the samples related to EP. This THz technique allows the use of larger spots compared to standard laser microscopy, higher accuracy in the pertinent range of roughness, and is compatible with in situ direct measurement of the EP process. As a whole, this study paves the way for non-destructive testing of AM devices and products, over large sample areas and in industrially relevant, safe environment. At the same time, it provides a useful tool for investigating the suitability of AM fabricated THz components.

2. Experimental results

2.1. Samples preparation and electrochemical polishing process

The unpolished samples were firstly prepared in a bi-dimensional square area of approximately 2.25 cm^2 large with a thickness of 0.2 cm by using the SLM AM technology. The 316 L stainless steel plates were anchored on the holder in the electrolyte by the mechanical support of an elastic gasket and screws during the polishing. The polishing procedure was finished in an electrochemical cell. Holder and electrochemical cell are shown in the Supplementary Information. The electrolyte was 1 mol/L NaCl-Ethylene Glycol (90%)-ethanol (10%) solution. After a standard EP process, the exposed metal surface was observed to be smoother. By holding the reaction temperature at room temperature via water bath and applying currents from

250 mA/cm^2 to 1000 mA/cm^2 of the polishing processes, the R_a of polished samples could be nicely controlled in the three ranges of 8-10 µm, 5-8 µm, and 1-5 µm, respectively [56].

2.2. THz-TDS mapping and average roughness evaluation

A commercial THz-TDS system (TERA K15, MenloSystems) configured in reflection geometry as presented in the Supplementary Information was used in this study to acquire the THz measurements. By raster scanning the sample and recording the sampled THz signals, a mapping of the reflected terahertz waveform can be produced. One of the main barriers for accurately extracting optical parameters in reflection THz-TDS is the sensitivity to phase misalignment between the sample and reference measurements. Thus, a particular care was used in precisely realigning the optical set-up in order to keep reference's and sample's surface in the focal plane. The flat sample used as the reference in these measurements was a 200 nm gold thin film on a

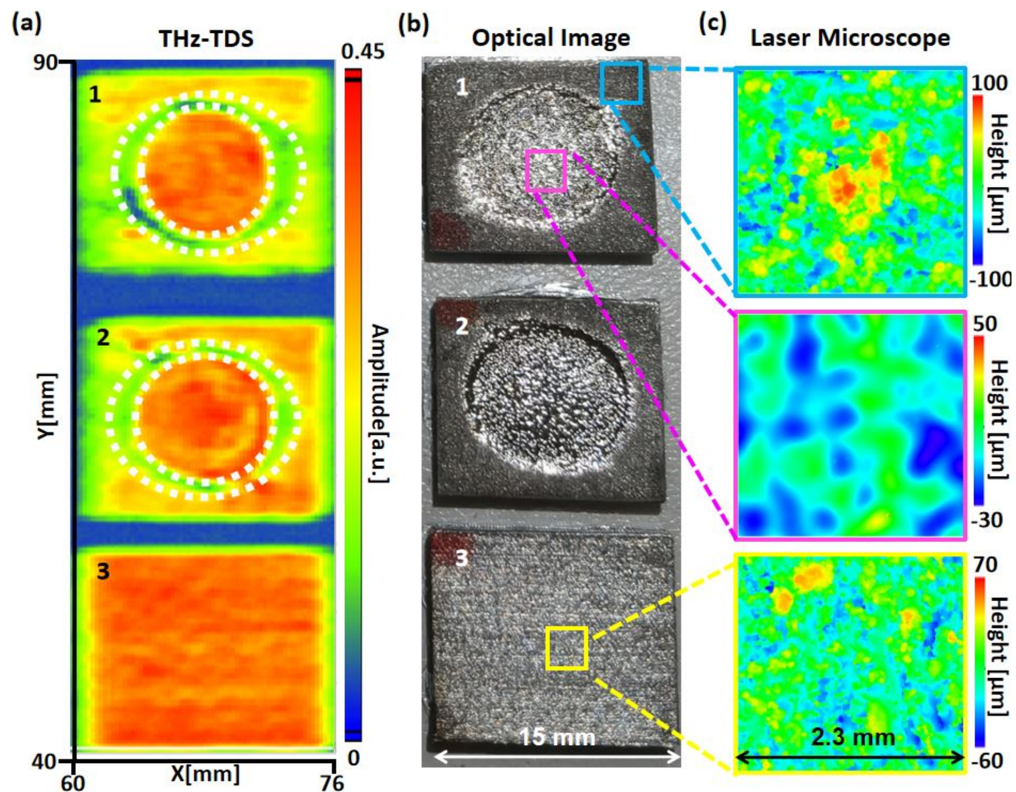

Fig. 1. (a) THz intensity mapping of three different samples acquired from reflection THz-TDS. The colorbar refers to the maximal reflected E-field of the time waveform. [Areas a-1, a-2]: Electrochemical-polished AM-printed samples, polished by 250 mA/cm^2 and 500 mA/cm^2 for 56 min, whose R_a in the central polished regions are in the range of 8-10 um and 5-8 um, respectively. [Area a-3]: An unpolished commercial metal plate. The white dash-dot circles label the partially polished ring region; (b) optical microscope images of the measured samples. [Areas b-1, b-2, b-3]: Samples corresponding to (a-1, a-2, a-3), respectively. The blue, pink and yellow squares represent the areas used for evaluating R_a via laser microscope in the unpolished, electrochemical-polished area of sample 1 and a random area in sample 3, respectively; (c) Height distribution images of the selected areas obtained by the laser microscope (the blue, pink and yellow frameworks correspond to the same areas shown in (b).

Optical Materials EXPRESS

500 µm Si substrate prepared by thermal evaporation. Two samples prepared using the SLM AM technology, and an extra commercial sample were investigated in this study, as shown in Fig. 1. The AM samples (samples 1 and 2) were polished via the electrochemical polishing cell. There are shiny circular regions in the centre of these samples that are nicely matched to the polishing holder shown in the Supplementary Information. Figure 1(a) shows the acquired intensity image from the THz-TDS, reporting the maximum reflected E-field as recorded by the THz-TDS system. The measured area has dimension of 16 mm (x) × 50 mm (y) and was acquired with a 0.25 mm step-size in both x and y directions. Each pixel in the image has a 100 ps-long digitalized THz time-domain information which has been averaged for 10 s. The image has very good contrast in reflection amplitude between the unpolished and polished areas in samples 1 and 2, as expected. Two highly reflective regions in the centre of samples 1 and 2 are found in the image which can be explained by the smoothened surface. The sample 3 area in the image has a more uniform reflection than samples 1 and 2. The higher average reflection of sample 3 compared to rough domains in samples 1 and 2 verify the rougher surface on the as-built AM component. In general, the reflection mapping shows a corresponding match to the roughness distribution in the optical image. However, two ring regions surrounding the smooth centres with low intensity (indicated by white dot lines), whose reflections are even smaller than the rough area, can be found in samples 1 and 2. The decrease in reflection is due to the uncompleted-polished sloping surface outside the polished region caused by unexpected electrolyte diffusion beyond the holder. The uneven surface changed the reflective angle of the incident THz wave, resulting in a minor reflection intensity acquired in the original direction. Thus, the collected information from these oblique areas will no longer be useful for evaluating the average roughness.

Three selected square regions with the size of 5.29 mm^2 from the unpolished, electrochemical-polished areas of sample and a random area of sample 3 (marked by blue, pink and yellow squares in the optical microscope picture of Fig. 1(b), respectively), individually, were investigated. Figure 1(c) shows the height distribution images of those three areas obtained by laser microscopy system, as described in the methods section. In the area after EP, its maximum and minimum relative heights were reduced and their uniformity was improved compared to the unpolished zone in the same sample, which are corresponding to the polishing effect on the surface as originally purposed. For matching the size of the scanning area of the laser microscope, the time-domain data of 81 pixels (9 × 9 in x and y directions) at the approximately same position were averaged and normalized by the reference acquired from the Au film. The typical time-domain waveforms and spectrums collected in the THz-TDS of the reference, polished flat area and unpolished rough area can be seen in the Supplementary Information.

2.3. Evaluating RMS roughness and height levelling of metal surface

In the images acquired from the THz-TDS introduced above, the relationship between the incident and the reflected THz wave in the specular direction can be expressed as Eq. (1) [57–59]:

$$E_r(\omega) = E_i(\omega) \cdot \tilde{f}(w; x, y) = E_i(\omega) \cdot r(\omega; x, y) = E_i(\omega) \cdot exp\frac{-i\omega\Delta H(x, y)}{c} \quad (1)$$

Where $E_i(\omega)$, $E_r(\omega)$ are the frequency-dependent electric field of the incident and reflected waves, respectively. $\tilde{f}(\omega; x, y)$ is the complex function expressing the changes of incident wave on the reflective surface, which is composed of the normalized reflective coefficient $r(\omega; x, y)$ and the phase item $exp[-i\omega\Delta H(x, y) / c]$. The phase contribution is caused by the height variation $\Delta H(x, y)$ of the sample's surface compared to the reference point. Considering that the height distribution on the sample surface is random, the correlation distance of the surface roughness is larger than the wavelength, and there is no phase delay caused by the surface's HL [8], the reflective coefficient $r(k)$ and reflectance $R(k)$ of the rough surface in the specular direction,

Optical Materials EXPRESS

which can be modelled by the Kirchhoff Approximation (*KA*) as given in equation (2-3) [60,61]:

$$r(k) = exp(-4\pi\sigma kcos\theta) \tag{2}$$

$$R(k) = (E_i / E_r)^2 = exp(-4\pi\sigma cos\theta)^2 \tag{3}$$

Where σ is the root-mean-squared (*RMS*) roughness, k is the wavenumber of the incident wave and θ is the incident angle with respect to the metallic surface normal vector. By investigating the electric field in the Fourier-transformed frequency domain, the R_a of the sample surface can be evaluated by Eq. (2) and the equation: $R_a = 0.8 \times \sigma$ [32]. The shadowing effect and multiple reflections among the surface caused by large incident angles are not considered in equations (2-3). However, *KA* is only valid while the *RMS* height is contributing significant diffuse scattering to the incident wavelength. The condition is often determined by the Fraunhofer Criterion as given in the inequality [33,61]:

$$\sigma \geq \frac{\lambda}{32\cos\theta} \tag{4}$$

where λ is the incident wavelength. This criterion is significant as it indicates the effective wavelength range for evaluating different R_a values. For example, a rough surface where

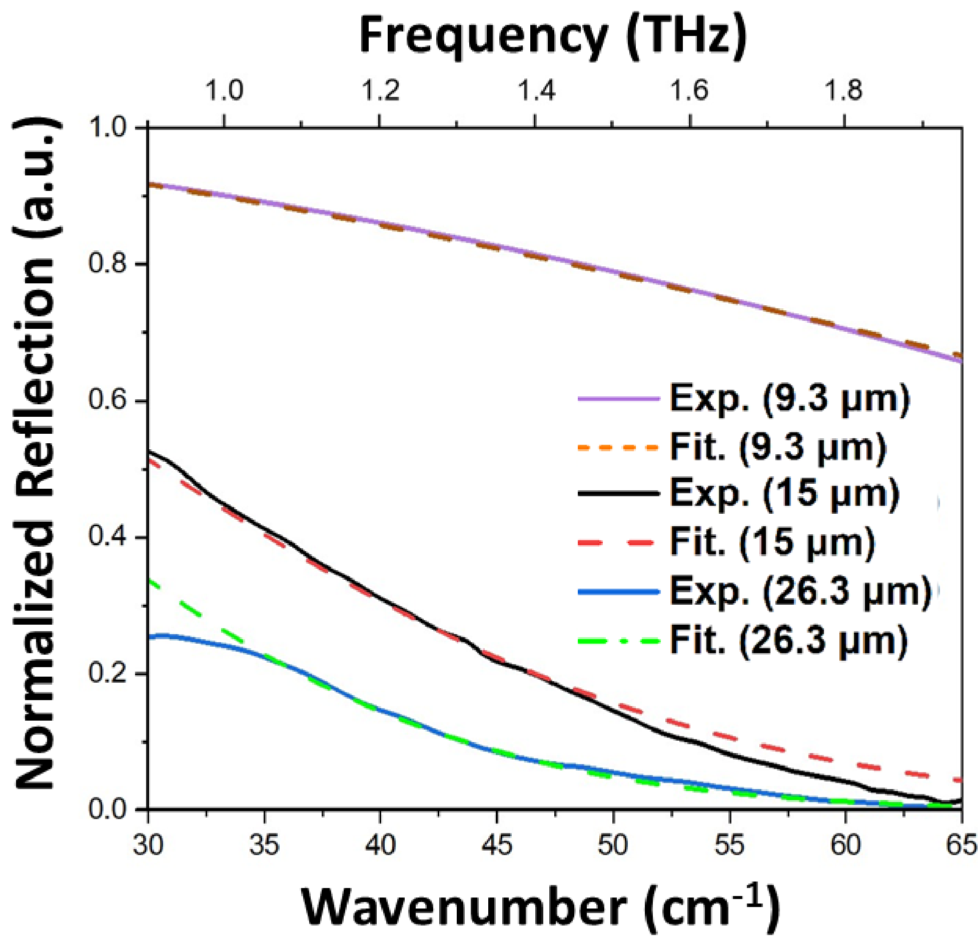

Fig. 2. Experimental results (Exp.) and fitting models (Fit.) of evaluating the average roughness of selected areas.

Optical Materials EXPRESS

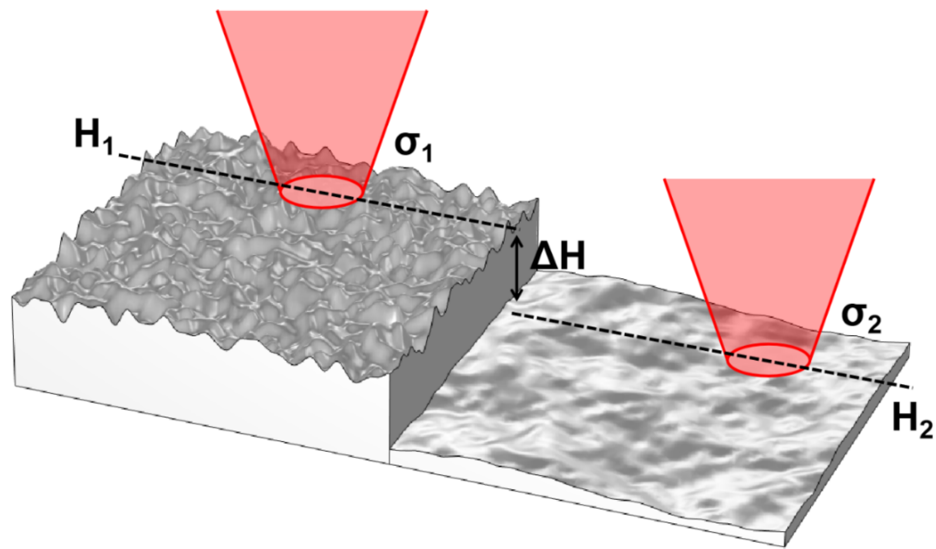

Fig. 3. Schematic of reflection THz-TDS used to characterize the different RMS roughness (σ) and HL in two identical areas, where $H_1 > H_2$ and $\sigma_1 > \sigma_2$. The left region represents the rough as-fabricated metal before EP, the right part represents the area after EP. The red round cones area represents the typical beam form of the incident THz pulse in THz-TDS.

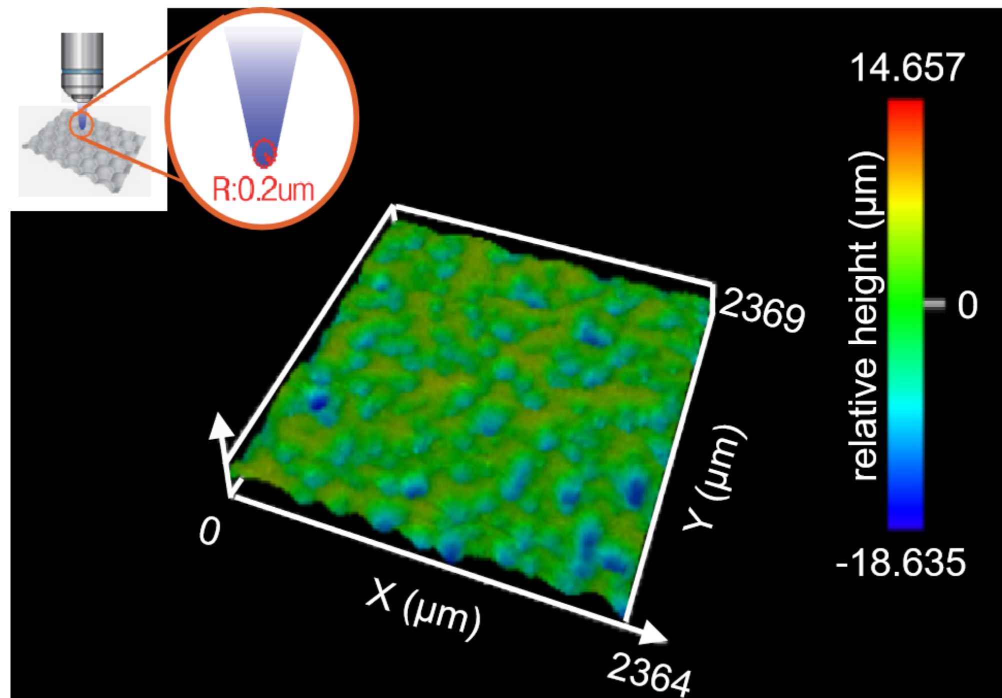

Fig. 4. Height distribution image measured by the laser microscope. (Inset: schematic of working principle of laser scanning microscope).

Optical Materials EXPRESS

$R_a = 40\,\mu m$ ($\sigma = 50\,\mu m$) usually can be retrieved by using KA with a spectral bandwidth from 0.2 THz to the highest readable frequency (2 THz in this measurement as shown in Supplementary Information). However, if a smoother surface where $R_a = 6\,\mu m$ ($\sigma = 7.5\,\mu m$) needs to be evaluated by the same method, the effective spectrum will be narrowed into the range from 1.5 THz to the end frequency which is close to the limit of the THz-TDS used in this measurement. From the normalized reflection, the R_a was evaluated by fitting the experimental data with Eq. (3) within the wavenumbers of 30-65 cm^{-1}. Figure 2 shows the experimental results and their best fits with the KA of the selected areas, evaluating the average roughness of 26.3 ± 2 μm, 9.3 ± 1 μm and 15 ± 2 μm, respectively. All fit models mentioned above are in good agreement with the experimental curves, resulting in a correlation coefficients R larger than 95%. In addition, in EP, the HL of the polished area will decrease with values $\Delta H(x, y)$ due to the continuous etching. The phase item in Eq. (1) caused by the height difference can effectively determine the actual etching depth on the surface. By integrating the R_a and the HL values evaluated from the THz-TDS, a 3D mapping characterising the EP process on the 3D-printed 316 L SS can be accomplished. The schematic of evaluating R_a and HL in two identical areas, where the left region represents raw 3D metal surface (rough and higher HL) and the region represents the area after the EP process (smooth and lower HL), can be seen in Fig. 3.

2.4. Laser scanning microscope measurements

THz-TDS results were validated against laser scanning microscope measurements. The average roughness evaluated from the laser scanning method was completed using an OLYMPUS OLS5000 Laser Scanning Microscope with an x20 objective, resulting in a spot radius of 0.2 μm on the sample surface as shown in the inset of Fig. 4. Figure 4 also shows a typical mapping of height distribution acquired by the laser writing. The RMS roughness was evaluated by:

$$R_a = \frac{1}{A} \iint_A |H(x, y)| \mathrm{d}x\mathrm{d}y \tag{5}$$

where A is the scanning area, H is the relative height to average leveling.

3. Comparison and critical discussion

Figure 5 shows the average roughness values of the investigated areas, evaluated by two strategies, laser microscope and THz-TDS. The accuracy standard of the laser microscope is in accordance with the ISO 25178-2:2012 certification, and the accuracy of the THz-TDS is calculated by the fitting model of the R values larger than 90%. The error bar obtained by THz-TDS method is larger than the one obtained by the laser system, and arises from the fitting procedure. However, the precision of THz-TDS measurements could be improved by acting on the S/N ratio of the system, e.g. by using parabolic mirrors with larger acceptance angle, by averaging more spatial and temporal waveforms, by implementing a vacuum experimental environment instead of nitrogen purging as in this work. A larger S/N, yielding a broader useful frequency spectral range, would allow the retrieval of μm or sub-μm roughness levels. The results are in very good agreement and demonstrate the use of THz-TDS as a promising way for the determination of the average roughness of AM components. The phase component $exp[-i\omega\Delta H(x, y) / c]$ can be isolated to evaluate the surface profile. Figure 6 (a) schematically present this measurement's acquisition procedure via THz-TDS scanning. During the measurement, the phase value of the initial point was set to 0, and the phase values of the succeeding points were recorded as the relative phase to the initial one. By fitting the phase difference, the frequency-dependent height differences can be determined. Figure 6(b) shows the partial surface profiles of sample 2 evaluated by two methods, THz-TDS and laser microscopy. The THz-TDS topography was calculated by the phase values at 1 THz of the data points. In the figure, the surface profile

Optical Materials EXPRESS

measured by THz-TDS has a very good match with the laser microscope. The ΔH measured by THz-TDS and laser microscope is 109 ± 2 μm and 108.61 ± 0.15 μm, respectively. There are three different areas that can be clearly classified from the profile acquired by both methods. These regions are (1) polished area, a terraced area whose relative height values are around 0 μm in the figure; (2) over-etched area, which is caused by the unexpected diffusion beneath the mechanical holder, resulting in a slope height profile from 0 μm to 110 μm according to the decreasing electric field from the exposed to the unexposed area; (3) Unpolished area, a terraced area whose relative values are around 110 μm in the figure. The varied surface profile measured by both methods are in good agreement with the effect of electrochemical polishing, validating THz-TDS as a useful way of evaluating surface profile of the electrochemical polished metal. However, there are two main factors affecting the resolution of this method: (1) Sampling rate of the time-domain information, 0.033ps in this measurement, corresponding to a height of 10 μm; (2) Diffraction and interaction limit of the applied THz pulse.

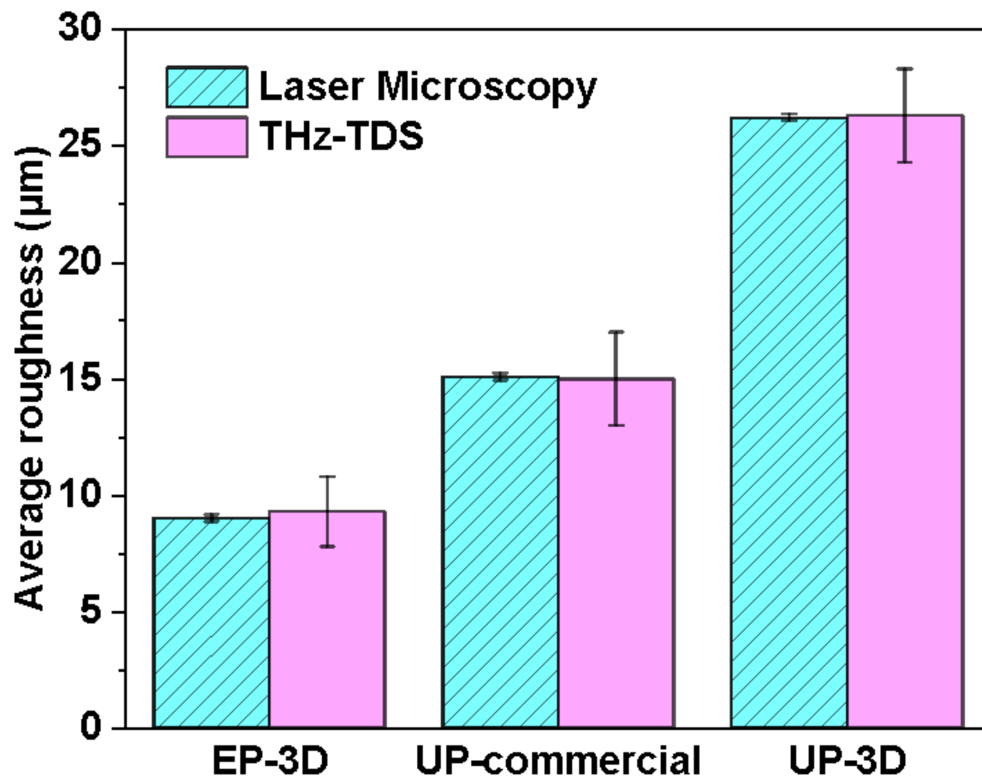

Fig. 5. Comparison of R_a of selected areas determined from the laser microscope and THz-TDS. EP-3D: electrochemical-polished area on AM fabricated sample, UP-3D: unpolished area on AM fabricated sample, UP-commercial: unpolished area on commercial sample.

The *HL* resolution is highly frequency-dependent in broadband THz-TDS, as the ΔH could be much smaller compared to some wavelengths in the broadband spectrum, thus introducing inaccuracy in the lower frequency components (up to 0.75 THz in this study). Accordingly, the phase values in this work were chosen in the range of 0.8-2 THz to ensure consistency. By integrating the *HL* and R_a information of all scanning pixels in the mapping, a 3D image with a size of 2×4.5 mm^2 evaluating R_a distribution and the surface profile was retrieved as displayed in Fig. 7. The lower plateau at the relative x position of 0 - 1500 μm is the same polished area illustrated in Fig. 1(b). The evaluated R_a values of the polished area are in the range of 6-11 μm,

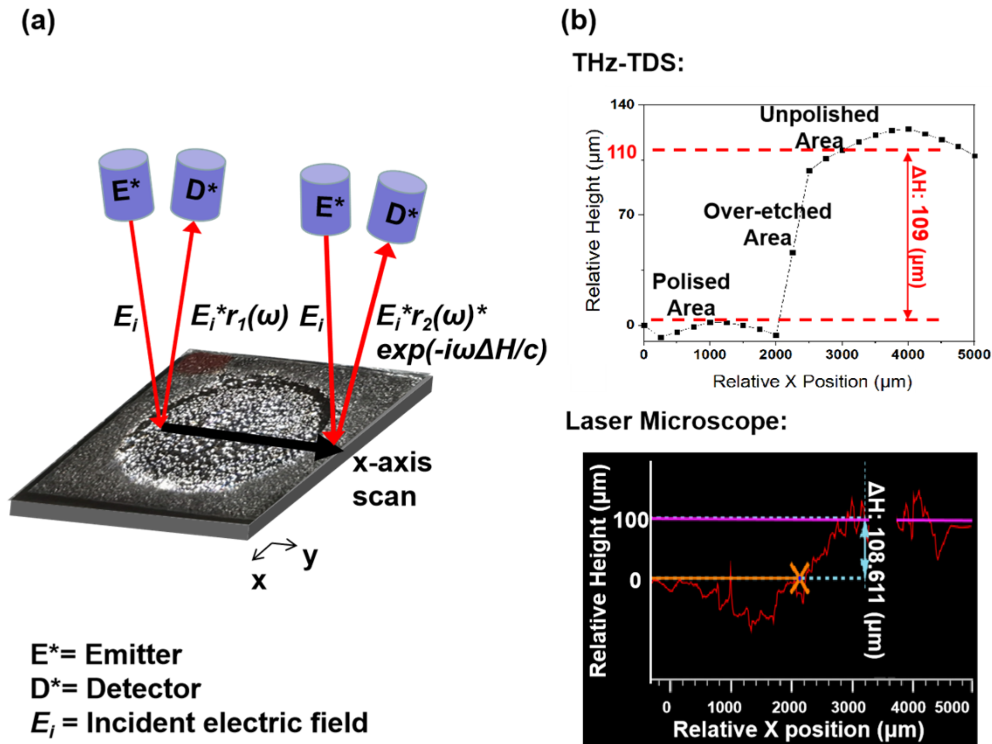

Fig. 6. (a) Schematic of *HL* evaluation based on phase change via THz-TDS (b) HL values measured from different techniques (top: THz-TDS, bottom: laser microscope). Three different (polished, over-etched, unpolished) regions can be classified by comparing the *HL* variances shown in the THz-TDS results.

which are consistent with the measurements shown in Fig. (2). Next to the polished area, a slope region located at the relative x position of 1500 - 2750 µm is the over-etched area. However, this area's high evaluated R_a values are not valid due to the changed incident angles on the slope surface distorting the *KA* fits. In the range of relative x positions 2750 - 4500 µm, the unpolished area with a higher terrace connected to the over-etched region can be spotted. Its R_a values are mainly located in the range of 25-35 µm, which is also in good agreement with the evaluation of the blue-framed area shown in Fig. (1). Generally, the R_a values and the height profile provided by this 3D image are consistent with the same information obtained from the laser microscope, demonstrating the suitability of THz-TDS for the evaluation of surface roughness and heights of EP AM fabricated components, as 316 L stainless steel for this case. Furthermore, considering the spot size in this study is approximately around 1 mm^2, the 0.25 mm step size of the images is oversampling. A comparison of the surface roughness and *HL* of a 4 mm^2 square area obtained via laser microscope and THz-TDS (with a step size of 1 mm) can be found in Table 1. In general, THz-TDS is an ideal method for evaluating samples where its R_a is in the range of 6-100 µm. It is the preferred method to work for large-scale scanning whose roughness needs to be considered beyond the millimetre range. Considering the semi-penetrating feature of the THz wave to non-conductive layers, it can be further utilized as a promising in-situ method to evaluate the EP process beneath the polishing cell.

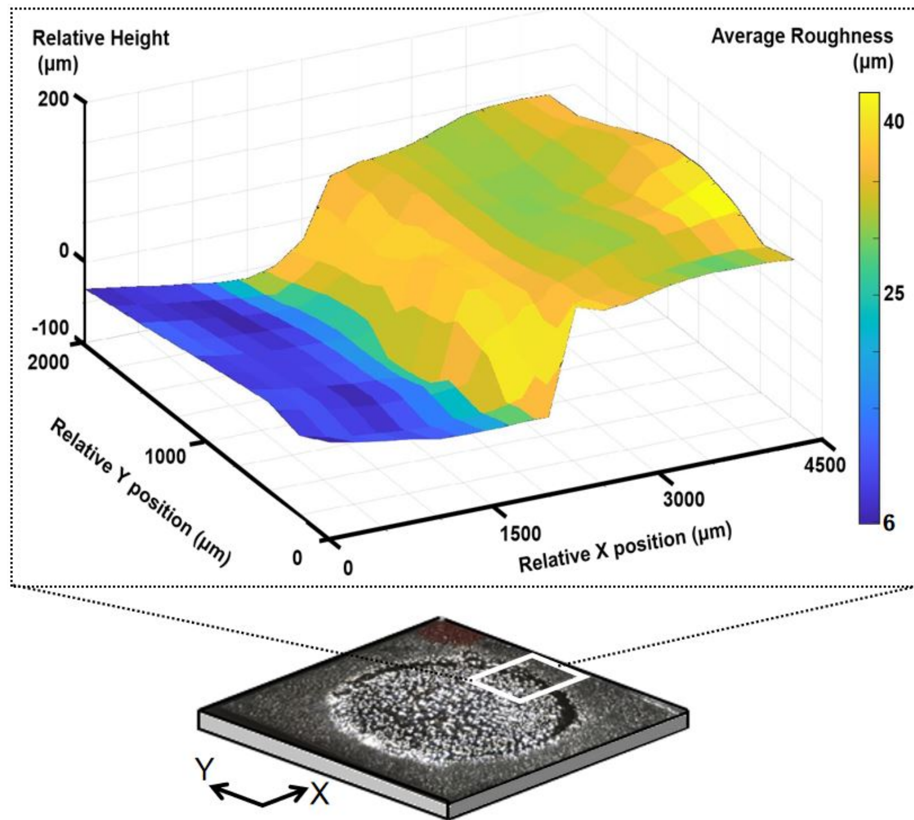

Fig. 7. 3D image of R_a and HL distribution (z-axis) of the partial surface of the sample 2.

Table 1. Comparison of R_a and HL of a 4 mm^2 square metallic area via laser microscopy and THz-TDS

	Laser microscopy	THz-TDS
Scanning time	5~10 mins, (it depends on the absolute roughness difference on the surface).	40 s (4 pixels with 10s averaging)
Data lost	Yes (for out-of-range peaks).	No
Resolution	0.2 μm	>1 mm
Confidence Range	>30 nm	>6 μm

4. Conclusion

In this study we investigated the R_a and HL distribution of the electrochemically polished AM fabricated components via THz-TDS spectroscopy and perform a comparison with laser microscopy technique. The experimental results show that THz-TDS can measure the average roughness and height profile of AM metallic surfaces with an excellent agreement with the state-of-art laser microscope. By integrating the information on roughness and height distribution, a 3D image demonstrating the metal surface profile was proposed. Compared to the laser microscope system, THz-TDS not only provide a safer environment but also quantitatively yields faster scans and error-free measurements, suggesting it is a more suitable technique to characterize the metal surface whose average roughness is in the range of 6-100 μm. Finally, these results

Optical Materials EXPRESS

allow to directly address the suitability of AM technique for the realization of THz building blocks such as waveguides or other integrated components.

Funding. Engineering and Physical Sciences Research Council (EP/R019460/1, EP/S019383/1); China Scholarship Council (CSC-202108890030).

Acknowledgements. HL acknowledges support from the Royal Academy of Engineering under the Industrial Fellowships program.

Disclosures. The authors declare no conflicts of interest.

Data availability. The datasets generated during the current study are openly available from Lancaster University's repository PURE, Ref. [62].

Supplemental document. See Supplement 1 for supporting content.

References

1. K.-E. Peiponen, J. A. Zeitler, and M. Kuwata-Gonokami, *Terahertz Spectroscopy and Imaging* (Springer, 2013).
2. J.-H. Son, *Terahertz Biomedical Science and Technology*, CRC Press, (2020).
3. H. Elayan, O. Amin, B. Shihada, R. M. Shubair, and M.-S. Alouini, "Terahertz band: The last piece of RF spectrum puzzle for communication," IEEE Open J. Commun. Soc. **1**, 1–32 (2020).
4. T. Nagatsuma, G. Ducournau, and C. Renaud, "Advances in terahertz communications accelerated by photonics," Nat. Photonics **10**(6), 371–379 (2016).
5. M. Naftaly, N. Vieweg, and A. Deninger, "Industrial Applications of Terahertz Sensing: State of Play," Sensors **19**(19), 4203 (2019).
6. D. Cimbri, J. Wang, A. Al-Khalidi, and E. Wasige, "Resonant tunnelling diodes high-speed terahertz wireless communications - a review," IEEE Trans. THz Sci. Technol. **12**(3), 226–244 (2022).
7. A. Khalatpour, A. K. Paulsen, and C. Deimert, *et al.*, "High-power portable terahertz laser systems," Nat. Photonics **15**(1), 16–20 (2021).
8. N. Vieweg, "Terahertz-time domain spectrometer with 90 dB peak dynamic range," J. Infrared, Millimeter, Terahertz Waves **35**(10), 823–832 (2014).
9. F. Ellrich, M. Bauer, N. Schreiner, A. Keil, T. Pfeiffer, J. Klier, S. Weber, J. Jonuscheit, F. Friederich, and D. Molter, "Terahertz Quality Inspection for Automotive and Aviation Industries," J. Infrared Millim. Terahertz Waves. **41**(4), 470–489 (2020).
10. D. Markl, A. Strobel, R. Schlossnikl, J. Bøtker, P. Bawuah, C. Ridgway, J. Rantanen, T. Rades, P. Gane, K.-E. Peiponen, and J. A. Zeitler, "Characterisation of pore structures of pharmaceutical tablets: A review," Int. J. Pharm. **538**(1-2), 188–214 (2018).
11. K. Ahi, S. Shahbazmohamadi, and N. Asadizanjani, "Quality control and authentication of packaged integrated circuits using enhanced-spatial-resolution terahertz time-domain spectroscopy and imaging," Opt. Lasers Eng. **104**, 274–284 (2018).
12. S. Rumyantsev, A. Muraviev, S. Rudin, G. Rupper, M. Reed, J. Suarez, and M. Shur, "Terahertz Beam Testing of Millimeter Wave Monolithic Integrated Circuits," IEEE Sensors J. **17**(17), 5487–5491 (2017).
13. M. Ma, Y. Wang, M. Navarro-Cía, F. Liu, F. Zhang, Z. Liu, Y. Li, S. M. Hanham, and Z. Hao, "The dielectric properties of some ceramic substrate materials at terahertz frequencies," J. Eur. Ceram. Soc. **39**(14), 4424–4428 (2019).
14. S. Engelbrecht, V. Pichot, T. Goepfert, H. Lin, and B. M. Fischer, "Extraction of Fickian water diffusion in polymers using terahertz time-domain spectroscopy," Polymer **257**, 125285 (2022).
15. H. Hoshina, Y Saito, T. Furuhashi, T. Shimazaki, M. Sawada, Y. Hioki, and C. Otani, "Terahertz spectroscopy for characterization of hydrogen bonding and cross-linked structure dynamics in polyurethane," J. Infrared Millim Terahertz Waves **41**(3), 265–275 (2020).
16. S. Nashima, O. Morikawa, K. Takata, and M. Hangyo, "Measurement of optical properties of highly doped silicon by terahertz time domain reflection spectroscopy," Appl. Phys. Lett. **79**(24), 3923–3925 (2001).
17. H. Lin, P. Braeuninger-Weimer, V. S. Kamboj, D. S. Jessop, R. Degl'Innocenti, H. E. Beere, D. A. Ritchie, J. A. Zeitler, and S. Hofmann, "Contactless graphene conductivity mapping on a wide range of substrates with terahertz time-domain reflection spectroscopy," Sci. Rep. **7**(1), 10625 (2017).
18. S. Wietzke, C. Jansen, M. Reuter, T. Jung, D. Kraft, S. Chatterjee, B. M. Fischer, and M. Koch, "Terahertz spectroscopy on polymers: A review of morphological studies," J. Mol. Struct. **1006**(1-3), 41–51 (2011).
19. H. Hoshina, S. Ishii, S. Yamamoto, Y. Morisawa, H. Sato, T. Uchiyama, Y. Ozaki, and C. Otani, "Terahertz spectroscopy in polymer research: assignment of intermolecular vibrational modes and structural characterization of poly (3-hydroxybutyrate)," IEEE Trans. THz Sci. Technol. **3**(3), 248–258 (2013).
20. M. C. Beard, G. M. Turner, and C. A. Schmuttenmaer, "Measuring intramolecular charge transfer via coherent generation of THz radiation," J. Phys. Chem. **106**(6), 878–883 (2002).
21. H. Lin, B. P. Russell, P. Bawuah, and J. A. Zeitler, "Sensing water absorption in hygrothermally aged epoxies with terahertz time-domain spectroscopy," Anal. Chem. **93**(4), 2449–2455 (2021).

22. Y. Yu, Z. Zhang, T. Zhang, X. Zhao, Y. Chen, C. Cao, Y. Li, and K. Xu, "Effects of surface roughness on terahertz transmission spectra," Opt. Quantum Electron. **52**(5), 240 (2020).
23. A. Jagannathan, A. J. Gatesman, and R. H. Giles, "Characterization of roughness parameters of metallic surfaces using terahertz reflection spectra," Opt. Lett. **34**(13), 1927–1929 (2009).
24. I. Cacciari and S. Siano, "Use of THz Reflectometry for Roughness Estimations of Archeological Metal Surfaces," J. Infrared Milli Terahz Waves **38**(4), 503–517 (2017).
25. T. Fukuchia, N. Fusea, M. Mizunob, and K. Fukunagab, "Surface Roughness Measurement Using Terahertz Waves," *Proceedings of the 3rd International Conference on Industrial Application Engineering* 294–299, (2015).
26. G. Sundberg, L. M. Zurk, S. Schecklman, and S. Henry, "Modeling Rough-Surface and Granular Scattering at Terahertz Frequencies Using the Finite-Difference Time-Domain Method," IEEE Trans. Geosci. Remote Sensing **48**(10), 3709–3719 (2010).
27. L. M. Zurk, S. C. Henry, S. Schecklman, and D. D. Duncan, "Physics-based processing for terahertz reflection spectroscopy and imaging," Infrared, Millimeter Wave, and Terahertz Technologies. Proc. SPIE **785403**, 785403 (2010).
28. M. Ortolani, J. S. Lee, U. Schade, and H.-W. Hübers, "Surface roughness effects on the terahertz reflectance of pure explosive materials," Appl. Phys. Lett. **93**(8), 081906 (2008).
29. M. H. Arbab, D. P. Winebrenner, E. I. Thorsos, and A. Chen, "Retrieval of terahertz spectroscopic signatures in the presence of rough surface scattering using wavelet methods," Appl. Phys. Lett. **97**(18), 181903 (2010).
30. S. Schecklman, L. M. Zurk, S. Henry, and G. P. Kniffin, "Terahertz material detection from diffuse surface scattering," J. Appl. Phys. **109**(9), 094902 (2011).
31. R. Burger, J Frisch, M. Hübner, M. Goldammer, O. Peters, E. Rönneberg, and D. Wu, "THz-TDS Reflection Measurement of Coating Thicknesses at Non-Perpendicular Incidence: Experiment and Simulation," Sensors **21**(10), 3473 (2021).
32. R. F. Anastasi and E. I. Madaras, "Terahertz NDE for metallic surface roughness evaluation. Nondestructive Evaluation and Health Monitoring of Aerospace Materials, Composites, and Civil Infrastructure," Proc. SPIE **61760O**, 61760O (2006).
33. F. T. Ulaby, R. K. Moore, and A. K. Fung, *Microwave Remote Sensing: Active and Passive: From Theory to Applications* (Artech House Publishers, 1986).
34. K. Sengupta, T. Nagatsuma, and D. M. Mittleman, "Terahertz integrated electronic and hybrid electronic–photonic systems," Nat. Electron. **1**, 622–635 (2018).
35. J. Dong, A. Tomasino, G. Balistreri, P. You, A. Vorobiov, É. Charette, B. Le Drogoff, M. Chaker, A. Yurtsever, S. Stivala, M. A. Vincenti, C. De Angelis, D. Kip, J. Azaña, and R. Morandotti, "Versatile metal-wire waveguides for broadband terahertz signal processing and multiplexing," Nat. Commun. **13**(1), 741 (2022).
36. Y. Li, Y. Wang, H. Li, B. Jiang, F. Bai, and J. Feng, "Terahertz Rectangular Waveguides by UV-LIGA with Megasonic Agitation," Micromachines **13**(10), 1601 (2022).
37. Y. Wang, X. Shang, and M. J. Lancaster, "Micromachined 3D millimeter-wave and terahertz devices," *2015 IEEE MTT-S International Microwave Workshop Series on Advanced Materials and Processes for RF and THz Applications (IMWS-AMP)*. 1–3 (2015).
38. R. Degl'Innocenti, Y. D. Shah, D. S. Jessop, Y. Ren, O. Mitrofanov, H. E. Beere, and D. A. Ritchie, "Hollow metallic waveguides integrated with terahertz quantum cascade lasers," Opt. Express **22**(20), 24439–24449 (2014).
39. W. Withayachumnankul, M. Fujita, and T. Nagatsuma, "Integrated Silicon Photonic Crystals Toward Terahertz Communications," Adv. Opt. Mater. **6**(16), 1800401 (2018).
40. W.J. Otter, N.M. Ridler, H. Yasukochi, K. Soeda, K. Konishi, J. Yumoto, M. Kuwata-Gonokami, and S. Lucyszyn, "3D printed 1.1 THz waveguides," Electron. Lett. **53**(7), 471–473 (2017).
41. J. Sun and F. Hu, "Three-dimensional printing technologies for terahertz applications: A review," Int J. RF Microw. Comput. Aided Eng. **30**, e21983 (2020).
42. S. T. Gassel, D. A. Azih, M. R. Hofmann, and C. Brenner, "Investigation of the Influence of Surface Roughness on Reflective THz Measurements," in *Proceedings of 47th International Conference on Infrared, Millimeter and Terahertz Waves (IRMMW-THz)*, (IEEE, 2022), pp. 1–2.
43. Y. Cao, K. Nallappan, H. Guerboukha, G. Xu, and M. Skorobogatiy, "Additive manufacturing of highly reconfigurable plasmonic circuits for terahertz communications," Optica **7**(9), 1112–1125 (2020).
44. Y. Ren, J. Du, B. Liu, Z. Jiao, Y. Tian, I. Baker, and H. Wu, "Microstructure, mechanical properties and biocompatibility of laser metal deposited Ti–23Nb coatings on a NiTi substrate," Mater. Sci. Eng., A **848**, 143402 (2022).
45. M. Yakout, M. Elbestawi, and S. C. Veldhuis, "Density and mechanical properties in selective laser melting of Invar 36 and stainless steel 316 L," J. Mater. Process. Technol. **266**, 397–420 (2019).
46. C. M. B. Ho, S. H. Ng, and Y.-J. Yoon, "A review on 3D printed bioimplants," Int. J. Precis. **16**(5), 1035–1046 (2015).
47. J. Muñoz and M. Pumera, "3D-printed biosensors for electrochemical and optical applications," Trends Analyt. Chem. **128**, 115933 (2020).
48. C. W. J. Lim, K. Q. Le, Q. Lu, and C. H. Wong, "An overview of 3-D printing in manufacturing, aerospace, and automotive industries," IEEE Potentials **35**(4), 18–22 (2016).
49. A. E. K. Mohammad and D. Wang, "Electrochemical mechanical polishing technology: recent developments and future research and industrial needs," Int. J. Adv. Manuf. Technol. **86**(5-8), 1909–1924 (2016).

Optical Materials EXPRESS

50. W. Han and F. Fang, "Fundamental aspects and recent developments in electropolishing," Int. J. Mach. Tools Manuf. **139**, 1–23 (2019).
51. E. Magsipoc, Q. Zhao, and G. Grasselli, "2D and 3D roughness characterization," Rock Mech. Rock Eng. **53**(3), 1495–1519 (2020).
52. W. Durham and B. Bonner, "PEAK: A new kind of surface microscope," Int. J. Rock Mech. Min. **30**(7), 699–702 (1993).
53. G. Kerckhofs, G. Pyka, M. Moesen, S. Van Bael, J. Schrooten, and M. Wevers, "High-resolution microfocus X-ray computed tomography for 3D surface roughness measurements of additive manufactured porous materials," Adv. Eng. Mater. **15**(3), 153–158 (2013).
54. R. De Oliveira, D. Albuquerque, T. Cruz, F. Yamaji, and F. Leite, *Measurement of the Nanoscale Roughness by Atomic Force Microscopy: Basic Principles and Applications. Atomic Force Microscopy-imaging, Measuring and Manipulating Surfaces at the Atomic Scale*, (IntechOpen, (2012).
55. A. Hongru, L. Xiangqin, S. Shuyan, Z. Ying, and L. Tianqing, "Measurement of Wenzel roughness factor by laser scanning confocal microscopy," RSC Adv. **7**(12), 7052–7059 (2017).
56. H. Zhu, A. Rennie, R. Li, and Y. Tian, "Two-Steps Electrochemical Polishing of Laser Powder Bed Fusion 316 L Stainless Steel," Surf. Interfaces **35**, 102442 (2022).
57. Y. Ino, J. Heroux, T. Mukaiyama, and M. Kuwata-Gonokami, "Reflection-type pulsed terahertz imaging with a phase-retrieval algorithm," Appl. Phys. Lett. **88**(4), 041114 (2006).
58. P. U. Jepsen, "Phase retrieval in terahertz time-domain measurements: a "how to" tutorial," J. Infrared Millim Terahertz Waves **40**(4), 395–411 (2019).
59. S. Van Frank, E. Leiss-Holzinger, M. Pfleger, and C. Rankl, "Terahertz time-domain polarimetry in reflection for film characterization," Sensors **20**(12), 3352 (2020).
60. E. I. Thorsos and D. R. Jackson, "The validity of the perturbation approximation for rough surface scattering using a Gaussian roughness spectrum," J. Acoust. Soc. Am. **86**(1), 261–277 (1989).
61. P. Beckmann and A. Spizzichino, *The Scattering of Electromagnetic Waves from Rough Surfaces* (Artech House Publishers, 1987).
62. Y. Lu, "Contactless 3D surface characterization of additive manufactured metallic components using terahertz time-domain spectroscopy: data," Lancaster University Research Directory, 2023, 10.17635/lancaster/researchdata/591.